Granular-Ball Computing-Based Fuzzy Twin Support Vector Machine for Pattern Classification

Guangming Lang, Lixi Zhao, Duoqian Miao, and Weiping Ding, *Senior Member, IEEE*

***Abstract*—The twin support vector machine (TWSVM) classifier and its fuzzy variant fuzzy twin support vector machine (FTSVM) have received considerable attention due to their low computational complexity. However, their performance often deteriorates when the input data is affected by noise. To overcome this limitation, this study leverages the robustness of granular-ball computing (GBC) against noise to develop more effective classification models by integrating GBC with TWSVM and FTSVM. First, we introduce the granular-ball TWSVM (GBTWSVM) classifier, which incorporates GBC with the TWSVM framework. By replacing traditional point-wise inputs with granular-ball representations, we derive a pair of nonparallel hyperplanes for the GBTWSVM classifier by solving a quadratic programming problem. Afterwards, we develop the granular-ball FTSVM (GBFTSVM) classifier, where the membership and nonmembership functions of granular-balls are defined using Pythagorean fuzzy sets, enabling a more nuanced differentiation of the contributions of granular-balls from distinct regions within the input space. By incorporating these functions into the FTSVM framework, we derive a pair of nonparallel hyperplanes for the GBFTSVM classifier through the solution of a quadratic programming problem. Finally, we present algorithms for the GBTWSVM and GBFTSVM classifiers and evaluate their performance on 21 benchmark datasets. Experimental results demonstrate the superior scalability, computational efficiency, and robustness of the proposed classifiers in pattern recognition, highlighting their potential as advanced tools for noise-tolerant classification.**

***Index Terms*—Fuzzy twin support vector machine (FTSVM), granular-ball computing, Pythagorean fuzzy sets (PFS), twin support vector machine (TWSVM).**

I. Introduction

Support vector machine (SVM), introduced by Vapnik in 1995 [1], is a foundational machine learning technique widely applied in both classification and regression tasks. Over the years, SVM and its numerous variants have demonstrated exceptional effectiveness in handling high-dimensional and nonlinear datasets [2], [3], [4], [5]. A particularly notable variant, twin SVM (TWSVM), differs from standard SVM by constructing two nonparallel hyperplanes for classification, rather than a single hyperplane [6], [7], [8], [9]. It ensures that each data point is closer to one hyperplane while being farther from the other. In classification tasks, new samples are assigned to the class associated with the nearest hyperplane. Furthermore, TWSVM achieves computational efficiency by solving two smaller-scale quadratic programming problems instead of a single large-scale problem. It retains the advantages of SVM in addressing high-dimensional and nonlinear problems while offering training speeds theoretically four times faster than the traditional SVM [10]. However, the performance of SVM and its variants often deteriorates when dealing with noisy datasets [11]. To mitigate the adverse effects of noise, researchers have developed the fuzzy SVM (FSVM) classifier, which assigns a membership degree to each sample based on its confidence within its native class [12], [13], [14], [15]. Although this membership-based approach enhances robustness, the membership functions of FSVM often rely solely on the distance between a sample and its class center, which may misidentify noisy data points far from the center as support vectors, thereby degrading classification performance. To address these limitations, numerous researchers have redefined the membership functions used in FSVM to improve its noise-resilience [16], [17], [18], [19], [20], [21]. For instance, Fan et al. introduced an entropy-based fuzzy membership function, leading to the development of the entropy-based fuzzy SVM (EFSVM) classifier [16]. Similarly, Rezvani, Wang, and Pourpanah [17] proposed the intuitionistic fuzzy twin SVM (IFTSVM) classifier, which integrates intuitionistic fuzzy sets into the TWSVM framework. These advancements not only enhance the robustness of SVM-based classifiers against noise but also improve their ability to accurately distinguish true support vectors from noisy or outlier samples, significantly advancing the state-of-the-art methods for classification tasks.

Granular computing (GC) is a computational paradigm that utilizes information granulation to process imprecise, inaccurate, and incomplete datasets. Zadeh [22] took vast amounts of information to achieve intelligent systems and controllers by leveraging the principles of GC. Since then, significant advancements have been made in integrating GC approaches including rough sets, fuzzy sets, three-way decisions, and formal

Received 2 December 2024; revised 1 March 2025; accepted 13 March 2025. Date of publication 21 March 2025; date of current version 3 July 2025. This work was supported in part by the National Key Research and Development Program of China under Grant 2022YFB3104700, in part by the National Natural Science Foundation of China under Grant 62076040, Grant 62376198, and Grant 12471431, in part by the Hunan Provincial Natural Science Foundation of China under Grant 2020JJ3034, and in part by the Scientific Research Fund of Hunan Provincial Education Department under Grant 22A0233. Recommended by Associate Editor J. Liu. *(Corresponding author: Weiping Ding.)*

Guangming Lang and Lixi Zhao are with the School of Mathematics and Statistics, Changsha University of Science and Technology, Changsha 410114, China (e-mail: langguangming1984@126.com; zhaolixi0915@163.com).

Duoqian Miao is with the School of Computer Science and Technology, Tongji University, Shanghai 201804, China (e-mail: dqmiao@tongji.edu.cn).

Weiping Ding is with the School of Artificial Intelligence and Computer Science, Nantong University, Nantong 226019, China, and also with the Faculty of Data Science, City University of Macau, Macau 999078, China (e-mail: dwp9988@163.com).

Digital Object Identifier 10.1109/TFUZZ.2025.3552281

concept analysis with machine learning [23], [24], [25], [26], [27], [28], [29], [30], [31]. Chen [32] pointed out that human cognition has the characteristic of large-scale priority. Inspired by this cognitive mechanism, Wang [33] proposed a framework of multigranularity cognitive computing to address uncertainty in information processing. Building upon this foundation, Xia et al. [34] introduced a novel method, namely, granular-ball computing, for deal with uncertain information, which merges the principles of granular computing with granular-ball representations, thereby offering a concrete methodology for information processing within the framework of granular computing. Afterwards, GBC has demonstrated strong applicability across various domains, including classification [34], [35], [36], [37], [38], [39], [40], [41], [42], clustering [43], [44], [45], [46], and attribute reduction [47], [48], [49], [50], [51], [52], [53], [54], [55]. Most recently, Xia et al. [38] proposed the granular-ball SVM (GBSVM) classifier, which integrates granular-balls with the SVM framework. Unlike traditional methods that treat individual samples as inputs, the GBSVM classifier utilizes granular-balls as inputs, representing a shift towards nonpoint input methods, and demonstrates significant robustness to noise and superior classification effectiveness. In practice, TWSVM outperforms standard SVM in classification accuracy and computational efficiency. Motivated by the robustness of GBC and the computational efficiency of TWSVM, this study aims to design a novel classifier by integrating granular-balls into the TWSVM framework, with the objective of constructing a model that exceeds GBSVM in both efficiency and effectiveness. Further progress has been achieved by Xue, Shao, and Xia [35], who introduced the granular-ball fuzzy SVM (GBFSVM) classifier. It offers enhanced robustness compared to the traditional FSVM approaches. However, the GBFSVM classifier faces limitations, as it determines the membership degree of granular-balls solely based on their distance from the class center. The granular-balls in boundary regions between two classes may receive identical membership degrees for both classes, which can lead to misclassifications and reduce the accuracy of predictions. Moreover, the current approach evaluates granular-ball memberships by calculating the Euclidean distance from the granular-ball's center to the sample class center, which risks overlooking support granular-balls located far from class centers but close to classification boundaries. Inspired by the robustness of GBC, the computational efficiency of TWSVM, and the flexibility of Pythagorean fuzzy sets (PFS) in handling uncertain problems, we aim to develop an improved classification framework that overcomes the limitations of GBFSVM. The contributions of this work are as follows.

1) We integrate GBC with the TWSVM framework to develop the GBTWSVM classifier. This novel classifier employs coarse-grained granular-balls as inputs, replacing traditional sample points. By positioning the hyperplane closer to one class of granular-balls while maintaining distance from the other class, the GBTWSVM classifier significantly enhances the robustness and efficiency of the TWSVM framework.
2) We combine GBC, PFS, and the FTSVM framework to propose the GBFTSVM classifier. This classifier introduces an innovative scoring function to assign differentiated scores to granular-balls located in positive and boundary regions. By capturing the distinct contributions of granular-balls across various regions, the GBFTSVM classifier further improves the performance of the GBTWSVM classifier.
3) We conduct a comprehensive evaluation of the GBTWSVM and GBFTSVM classifiers on 21 benchmark datasets from the UCI Machine Learning Repository. The experimental results reveal that both classifiers outperform seven state-of-the-art classification methods across multiple metrics, including running time, accuracy, precision, and recall. Notably, the GBTWSVM and GBFTSVM classifiers exhibit superior robustness against noise, underscoring their effectiveness in real-world classification tasks.

The rest of this article is organized as follows. Section II provides a review of GBC, TWSVM, and FSVM. Section III develops the GBTWSVM classifier. Section IV presents the GBFTSVM classifier. Section V reports experimental results with the GBTWSVM and GBFTSVM classifiers. Finally, Section VI concludes this article.

II. Preliminaries

In this section, we review some concepts of GBC [34], TWSVM [6], and FSVM [12].

A. Granular-Ball Computing

The fundamental concept of GBC involves utilizing a family of granular-balls to cover the original dataset, replacing individual sample points with granular-balls as computational inputs. Consider a dataset $U = \{(x_1, l_1), (x_2, l_2), \ldots, (x_n, l_n)\}$, where $X = \{x_k \mid x_k \in \mathcal{R}^d,\ k = 1, 2, \ldots, n\}$ stands for the feature value matrix of U with d features, and $\mathcal{L} = \{l_k \mid l_k \in \mathcal{R},\ k = 1, 2, \ldots, n\}$ is the corresponding label vector. The sample universe U is covered by a family of granular-balls $\mathcal{GB} = \{GB_i \mid i = 1, 2, \ldots, m\}$. The center of the ith granular-ball GB_i is calculated as $c_i = \frac{1}{n_i}\sum_{k=1}^{n_i} x_{ik}$, where x_{ik} represents the ikth sample and n_i is the number of samples within GB_i. There are two available methods to determine the radius r_i of the granular-ball GB_i: $r_i = \max_{x_{ik} \in GB_i} |x_{ik} - c_i|$ and $r_i = \frac{1}{n_i}\sum_{k=1}^{n_i} |x_{ik} - c_i|$, and in this study, we adopt the average distance as the radius of the granular-ball. To eliminate the effect of noisy data within each granular-ball, the overall label $y_i = \arg\max_{l_k \in \mathcal{L}} \mid \{(x, l) \in GB_i \mid l = l_k\} \mid$ of GB_i takes the label that appears most frequently within the granular-ball. The purity $p_i = \frac{|\{(x,l) \in GB_i | l = y_i\}|}{n_i}$ denotes the proportion of samples with the label y_i in GB_i. This metric quantifies the consistency of sample labels within each granular-ball. In fact, granular-balls can be regarded as adaptive neighborhoods, where their centers and radii are determined through optimization methods, enabling them to accurately capture the local structure of the data. Compared to the traditional neighborhoods, granular-balls exhibit greater adaptability and flexibility, making them more effective in representing complex data.

In GBC, the initial primary objective is to generate a family of granular-balls $\mathcal{GB}$ that effectively encapsulates the dataset. The objective function for granular-ball generation is formulated as

$$\min \quad \lambda_1 \times \frac{n}{\sum_{GB_i \in \mathcal{GB}} |GB_i|} + \lambda_2 \times m, \tag{1}$$

$$\text{s.t.} \quad quality(GB_i) \geq T \tag{2}$$

where λ_1 and λ_2 are weight coefficients, m is the total number of granular-balls, and $quality(GB_i)$ represents the proportion of the majority of samples with the same label in the granular-ball GB_i. However, the traditional methods of generating granular-balls encounter challenges in adapting to the unique data distribution of each dataset. These challenges primarily stem from the difficulty in setting a fixed purity threshold parameter that aligns with diverse dataset characteristics. To address this limitation, Xia et al. [37] proposed a purity-adaptive method of granular-ball generation, and made the granular-ball generation completely parameter-free. The objective function can be expressed as follows:

$$\begin{aligned} \min \quad & \lambda_1 \times \frac{n}{\sum_{GB_i \in \mathcal{GB}} |GB_i|} + \lambda_2 \times m, \\ \text{s.t.} \quad & quality(GB_i) \geq T_0, W(\mathcal{GB}_i) > quality(GB_i), \\ & \|c_i - c_j\| > \|r_i - r_j\| (i, j \in [1, m], y_i \neq y_j) \end{aligned} \tag{3}$$

where T_0 stands for the initial purity of the granular-ball, $\mathcal{GB}_i$ denotes the set of the child granular-balls of GB_i, and $W(\mathcal{GB}_i)$ signifies the weighted sum of purities of the child granular-balls of GB_i. This adaptive approach ensures that the granular-ball generation process dynamically aligns with the underlying data distribution, thereby enhancing robustness and eliminating reliance on prespecified purity parameters.

B. TWSVM and FSVM

The TWSVM classifier aims to find a pair of nonparallel hyperplanes, with each hyperplane positioned closer to samples of its corresponding class while maintaining a certain distance from samples of the opposite class. A new sample $x \in \mathcal{R}^d$ is assigned to class $+1$ or -1 depending on which hyperplane it is closest to. The pair of nonparallel hyperplanes of the TWSVM classifier is derived by solving the following quadratic programming problems (QPPs):

$$\begin{aligned} \min_{\omega_1, b_1, \xi_2} \quad & \frac{1}{2}(x_A\omega_1 + e_1 b_1)^T (x_A\omega_1 + e_1 b_1) + C_1 e_2^T \xi_2, \\ \text{s.t.} \quad & -(x_B\omega_1 + e_2 b_1) + \xi_2 \geq e_2, \xi_2 \geq 0, \end{aligned} \tag{4}$$

and

$$\begin{aligned} \min_{\omega_2, b_2, \xi_1} \quad & \frac{1}{2}(x_B\omega_2 + e_2 b_2)^T (x_B\omega_2 + e_2 b_2) + C_2 e_1^T \xi_1, \\ \text{s.t.} \quad & (x_A\omega_2 + e_1 b_2) + \xi_1 \geq e_1, \xi_1 \geq 0 \end{aligned} \tag{5}$$

where matrices x_A and x_B stand for the samples of classes +1 and -1, respectively, C_1 and C_2 are penalty parameters, e_1 and e_2 are vectors of ones with suitable dimensions, and ξ_1 and ξ_2 are slack variables.

In the dual form, the pair of nonparallel hyperplanes is derived by solving the following QPPs:

$$\begin{aligned} \max_{\alpha} \quad & \alpha^T e_2 - \frac{1}{2}\alpha^T G(H^T H)^{-1} G^T \alpha, \\ \text{s.t.} \quad & 0 \leq \alpha \leq C_1 \end{aligned} \tag{6}$$

and

$$\begin{aligned} \max_{\gamma} \quad & \gamma^T e_1 - \frac{1}{2}\gamma^T P(Q^T Q)^{-1} P^T \gamma, \\ \text{s.t.} \quad & 0 \leq \gamma \leq C_2 \end{aligned} \tag{7}$$

where $H = [x_A \quad e_1]$, $G = [x_B \quad e_2]$, $P = [x_A \quad e_1]$, $Q = [x_B \quad e_2]$, $u = [\omega_1 \quad b_1]^T = (H^T H)^{-1} G^T \alpha$, and $v = [\omega_2 \quad b_2]^T = (Q^T Q)^{-1} P^T \gamma$.

Assume a training dataset $\widetilde{U} = \{(x_1, l_1, s_1), (x_2, l_2, s_2), \ldots, (x_n, l_n, s_n)\}$, where $s_k \in (0, 1]$ is the membership degree of x_k to its corresponding label l_k. The FSVM classifier seeks to determine an optimal hyperplane by solving the following optimization problem:

$$\begin{aligned} \min \quad & \frac{1}{2}\|\omega\|^2 + C \sum_{k=1}^{n} s_k \xi_k, \\ \text{s.t.} \quad & l_k(\omega^T \phi(x_k) + b) \geq 1 - \xi_k, \\ & \xi_k \geq 0, k = 1, 2, \ldots, n \end{aligned} \tag{8}$$

where C is a penalty parameter, ξ_k is a slack variable, and $\phi(x_k)$ represents the mapping to a higher-dimensional space. This formulation incorporates membership degrees to reduce the impact of noise on the hyperplane's placement.

III. Granular-Ball Twin Support Vector Machine

In this section, we detail the construction of the GBTWSVM classifier and present the corresponding algorithm for its application in classification tasks [41]. The framework for constructing the GBTWSVM classifier is illustrated in Fig. 1.

We define two nonparallel hyperplanes $f_1(x) : x^T\omega_1 + b_1 = 0$ and $f_2(x) : x^T\omega_2 + b_2 = 0$, where $f_1(x)$ stands for the hyperplane close to the positive-class granular-ball ($y_i = +1$), and $f_2(x)$ stands for the hyperplane close to the negative-class granular-ball ($y_i = -1$). Here, ω_t and b_t denote the normal vector and bias of $f_t(x)$, respectively, where $t \in \{1, 2\}$. The two hyperplanes are constrained by the following principles: 1) each hyperplane should be as close as possible to the center of the granular-balls of its respective class and 2) each hyperplane should maintain the maximum possible distance from the surfaces of the granular-balls belonging to the opposite class. For binary classification problems, assume m_1 granular-balls of class $+1$ and m_2 granular-balls of class -1 are generated. The centers of the granular-balls of classes $+1$ and -1 are represented by the matrices c_A and c_B, respectively, while their radii of the granular-balls of classes $+1$ and -1 are represented by the

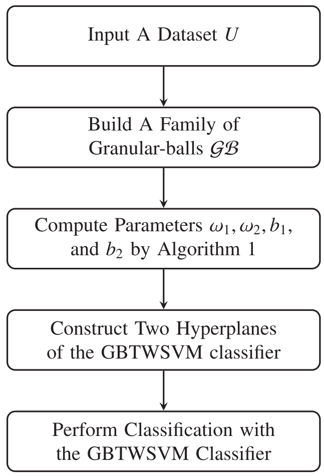

Fig. 1. Framework of the GBTWSVM classifier.

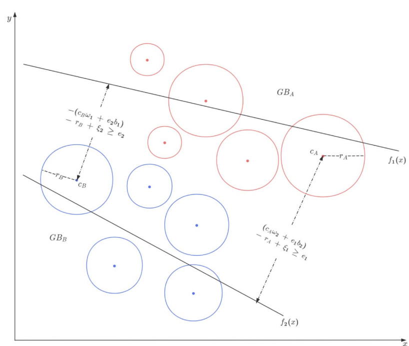

Fig. 2. GBTWSVM classifier.

matrices r_A and r_B, respectively. The graphical representation of the GBTWSVM classifier is illustrated in Fig. 2, where the red and blue circles represent granular-balls of class $+1$ and class -1, respectively. A pair of nonparallel hyperplanes of the GBTWSVM classifier is derived by solving the following QPPs:

$$\min_{\omega_1, b_1, \xi_2} \ \frac{1}{2}(c_A\omega_1 + e_1 b_1)^T (c_A\omega_1 + e_1 b_1) + C_1 e_2^T \xi_2,$$
$$\text{s.t.} \quad -(c_B\omega_1 + e_2 b_1) - r_B + \xi_2 \geq e_2, \xi_2 \geq 0 \tag{9}$$

and

$$\min_{\omega_2, b_2, \xi_1} \ \frac{1}{2}(c_B\omega_2 + e_2 b_2)^T (c_B\omega_2 + e_2 b_2) + C_2 e_1^T \xi_1,$$
$$\text{s.t.} \quad (c_A\omega_2 + e_1 b_2) - r_A + \xi_1 \geq e_1, \xi_1 \geq 0 \tag{10}$$

where C_1 and C_2 are positive penalty parameters, and e_1 and e_2 are unit vectors with appropriate dimensions.

The GBTWSVM classifier minimizes the structural risk by incorporating the regularization term to the margin maximization objective. This objective is formulated as a pair of QPPs, which can be addressed through the corresponding Lagrange function:

$$\begin{aligned} &L(\omega_1, b_1, \xi_2, \alpha, \beta) \\ &= \frac{1}{2}\|c_A\omega_1 + e_1 b_1\|^2 + C_1 e_2^T \xi_2 - \alpha^T(-(c_B\omega_1 + e_2 b_1) \\ &\quad + \xi_2 - r_B - e_2) - \beta^T \xi_2 \end{aligned} \tag{11}$$

where α and β are Lagrangian multipliers. This formulation integrates the optimization of hyperplane placement while accounting for the tradeoff between minimizing classification error and maximizing margin, thus enhancing the generalization capability of the classifier.

According to the Karush–Kuhn–Tucker (KKT) conditions, the Lagrange function must satisfy the following conditions:

$$\frac{\partial L}{\partial \omega_1} = c_A^T(c_A\omega_1 + e_1 b_1) + c_B^T \alpha = 0; \tag{12}$$

$$\frac{\partial L}{\partial b_1} = e_1^T(c_A\omega_1 + e_1 b_1) + e_2^T \alpha = 0; \tag{13}$$

$$\frac{\partial L}{\partial \xi_2} = C_1 e_2^T - \alpha - \beta = 0. \tag{14}$$

By combining (12) and (13), we arrive at the following matrix formulation:

$$\begin{bmatrix} c_A^T \\ e_1^T \end{bmatrix} \begin{bmatrix} c_A & e_1 \end{bmatrix} \begin{bmatrix} \omega_1 \\ b_1 \end{bmatrix} + \begin{bmatrix} c_B^T \\ e_2^T \end{bmatrix} \alpha = 0. \tag{15}$$

Let $E = [c_A \quad e_1]$, $F = [c_B \quad e_2]$, and $u = [\omega_1 \quad b_1]^T$. Using these notations, (15) can be rewritten as

$$E^T E u + F^T \alpha = 0. \tag{16}$$

To improve its generalization capacity, we add a regularization item, and get the expression of u

$$u = -(E^T E + \varepsilon I)^{-1} F^T \alpha. \tag{17}$$

Similarly, for the second hyperplane, let $R = [c_A \quad e_1]$, $S = [c_B \quad e_2]$, and $v = [\omega_2 \quad b_2]^T$, we get the expression of v

$$v = (S^T S + \varepsilon I)^{-1} R^T \gamma. \tag{18}$$

A pair of nonparallel hyperplanes for the dual model of the GBTWSVM classifier is obtained by solving the following QPPs:

$$\max_{\alpha} \ \alpha^T(e_2 + r_B) - \frac{1}{2}\alpha^T F(E^T E)^{-1} F^T \alpha,$$
$$\text{s.t.} \quad 0 \leq \alpha \leq C_1 \tag{19}$$

and

$$\max_{\gamma} \ \gamma^T(e_1 + r_A) - \frac{1}{2}\gamma^T R(S^T S)^{-1} R^T \gamma,$$
$$\text{s.t.} \quad 0 \leq \gamma \leq C_2. \tag{20}$$

For a new sample $x \,\epsilon\, \mathcal{R}^d$, the class label $t \in \{1, 2\}$ is determined by comparing the distances between the sample and the two hyperplanes. Specifically, the sample is assigned to the class corresponding to the closest hyperplane

$$\text{Class}\, t = arg\ \min_{t \in \{1,2\}} \frac{|\langle \omega_t, x\rangle + b_t|}{\|\omega_t\|}. \tag{21}$$

This decision rule ensures that the new sample is assigned to the class associated with the nearest hyperplane, thereby leveraging the granular-ball proximity information for accurate classification.

The algorithm for constructing the GBTWSVM classifier is presented as follows.

Algorithm 1: GBTWSVM Classifier.

```
Input: Granular-balls
  GB = {(c_i, r_i, p_i, y_i) | i = 1, 2, ..., m}.
Output: Hyperplane parameters ω1, ω2, b1, and b2.
Initialize c_A, c_B, r_A, and r_B as empty matrices;
for each GB_i ∈ GB do
  if y_i = +1 then
    add c_i to c_A and r_i to r_A;
  else
    add c_i to c_B and r_i to r_B;
  end if
end for
Use (19) and (20) to define the dual quadratic
  programming problems;
Perform L-BFGS-B optimization to compute the
  Lagrange multipliers α and γ;
Calculate ω1 and b1 for the first hyperplane by (17);
Calculate ω2 and b2 for the second hyperplane by (18);
return Hyperplane parameters ω1, ω2, b1, and b2.
```

Suppose the training dataset consist of n samples, with approximately $n/2$ samples per class, the time complexity of SVM is $O(n^3)$, which scales cubically with the number of training samples. In contrast, the time complexity of TWSVM is $O(2 \times (n/2)^3)$, which is four times faster than SVM. If n samples generate m granular-balls ($m < n$), with each class having approximately $m/2$ granular-balls, the time complexity of GBTWSVM is $O(2 \times (m/2)^3)$. If the number of generated granular-balls $m \approx n/2$, the computational speed of GBTWSVM is eight times faster than TWSVM due to its reliance on a reduced number of granular-balls. The enhanced efficiency makes GBTWSVM particularly well suited for large-scale classification tasks, effectively balancing computational cost with classification performance.

IV. Granular-Ball Fuzzy Twin Support Vector Machine

In this section, we present a detailed account of the construction of the GBFTSVM classifier along with its associated algorithm for effective implementation in classification tasks. The framework for constructing the GBFTSVM classifier is depicted in Fig. 3.

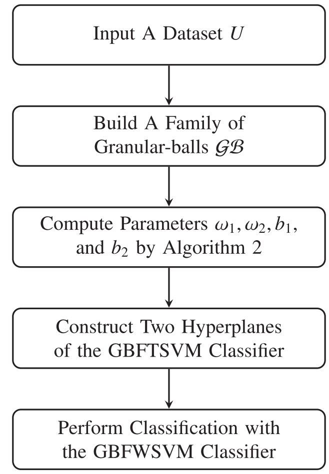

Fig. 3. Framework of the GBFTSVM classifier.

A. Pythagorean Fuzzy Membership Assignment

Assume $X = \{x_k \mid k = 1, 2, \ldots, n\}$ is a dataset with n sample points, from which a set of granular-balls $\mathcal{GB} = \{GB_i \mid i = 1, 2, \ldots, m\}$ is derived. Each granular-ball GB_i is assigned a pair of membership and nonmembership degrees (μ_{GB_i}, ν_{GB_i}), such that $0 \leq \mu_{GB_i}, \nu_{GB_i} \leq 1$ and $\mu_{GB_i}^2 + \nu_{GB_i}^2 \leq 1$. These degrees characterize the relationship between the granular-ball GB_i and a specific class. Let $\mu_P(x_{ik})$ and $\nu_P(x_{ik})$ represent the membership and nonmembership degrees of a sample x_{ik} in a given class, respectively, then the membership and nonmembership degrees of the granular-ball GB_i in that class are defined by

$$\mu_{GB_i} = \frac{1}{n_i} \sum_{k=1}^{n_i} \mu_P(x_{ik}), \nu_{GB_i} = \frac{1}{n_i} \sum_{k=1}^{n_i} \nu_P(x_{ik}) \tag{22}$$

where x_{ik} is the ikth sample within the ith granular-ball GB_i, and n_i denotes the number of samples in GB_i. In most cases, the membership and nonmembership degrees of individual samples are not directly known. So, we design the membership and nonmembership functions of the granular-balls as follows.

1) *Membership Degree:* The majority of methods for constructing membership functions rely on the distance between individual samples and their respective class centers. For binary-class granular-balls $\mathcal{GB} = \{(c_i, r_i, p_i, y_i) \mid 1 \leq i \leq m\}$, where c_i, r_i, p_i, and y_i represent the center, radius, purity, and label of GB_i, respectively, the class center C^+ and the maximum radius R^+ of positive-class granular-balls ($y_i = +1$), as well as the class center C^- and the maximum radius R^- of negative-class granular-balls ($y_i = -1$), are defined as

$$C^+ = \frac{1}{m_+} \sum_{y_i=+1} c_i, R^+ = \max_{y_i=+1} \left\| c_i - C^+ \right\|; \tag{23}$$

$$C^- = \frac{1}{m_-} \sum_{y_i=-1} c_i, R^- = \max_{y_i=-1} \left\| c_i - C^- \right\| \tag{24}$$

where m_+ and m_- stand for the numbers of positive and negative granular-balls, respectively. For a granular-ball GB_i, the membership degree can be defined as

$$\mu_{GB_i} = \begin{cases} 1 - \frac{\left\| c_i - C^+ \right\|}{R^+ + \varepsilon}, & \text{if } y_i = +1; \\ 1 - \frac{\left\| c_i - C^- \right\|}{R^- + \varepsilon}, & \text{if } y_i = -1 \end{cases} \tag{25}$$

where ε is a small positive constant.

2) *Nonmembership Degree:* Utilizing the membership degree and the purity of a granular-ball GB_i, we give the nonmembership degree as follows:

$$\nu_{GB_i} = \sqrt{(1 - \mu_{GB_i}^2)(1 - p_i)} \tag{26}$$

where p_i indicates the purity of GB_i. For each granular-ball GB_i, the membership degree μ_{GB_i} and the non-membership degree ν_{GB_i} satisfy the conditions: $0 < \mu_{GB_i}, \nu_{GB_i} \leq 1$, and $0 \leq \mu_{GB_i}^2 + \nu_{GB_i}^2 \leq 1$.

Remark: Pythagorean fuzzy sets [56], [57], [58] extend intuitionistic fuzzy sets, offering greater flexibility in handling uncertainty and fuzziness. Accordingly, this study employs Pythagorean fuzzy sets to define the membership and non-membership degrees of granular-balls. Furthermore, the positive constant ε ensures that the membership degree of a granular-ball containing a single object remains meaningful, and cannot overly affect the values of the membership function. Therefore, a small positive value, such as 0.0001 or 0.00001, can be appropriately selected.

In three-way decisions, Yao [59] categorized objects into three distinct groups based on their evaluations to minimize the risk of misclassification. Specifically, objects with different evaluations are assigned to different regions. Analogously, the impact of individual samples on classification is not uniform. The samples located in the boundary region play a crucial role in achieving accurate classifications. Conversely, the samples situated farther from the boundary contribute relatively less to the classification. To accurately measure the contribution of granular-balls in various regions to classification, we categorize them into positive and boundary regions, and assign them different scoring functions. Based on the closeness index of PFS, we define the granular-ball closeness function as follows:

$$\theta_{GB_i} = \sqrt{\frac{1-\nu_{GB_i}^2}{2-\mu_{GB_i}^2-\nu_{GB_i}^2}}. \tag{27}$$

In classification tasks, granular-balls positioned in the boundary region are typically close to the decision boundary, playing a significant role in its determination. In contrast, granular-balls located in the positive region are generally farther from the decision boundary and have little influence on its construction. According to the theory of three-way decisions, if the purity of granular-ball GB_i equals 1, then GB_i belongs to the positive region. If the purity of granular-ball GB_i is not equal to 1, then GB_i belongs to the boundary region. To reflect these differences in contribution, we assign a lower score μ_{GB_i} to the granular-ball in the positive region and a higher score θ_{GB_i} to that in the boundary region. The scoring function of the granular-ball GB_i is defined as follows:

$$s_{GB_i} = \begin{cases} \mu_{GB_i}, & \text{if } p_i = 1; \\ \theta_{GB_i}, & \text{if } p_i \neq 1. \end{cases} \tag{28}$$

In Fig. 4, dashed granular-balls stand for those belonging to the boundary region, typically positioned close to the separating boundary, and are assigned a higher score. In contrast, solid granular-balls stand for those belonging to the positive region, and they are often positioned far from the separating boundary. This scoring function effectively distinguishes the contributions of granular-balls in different regions, offering a more nuanced understanding of their roles in the classification process.

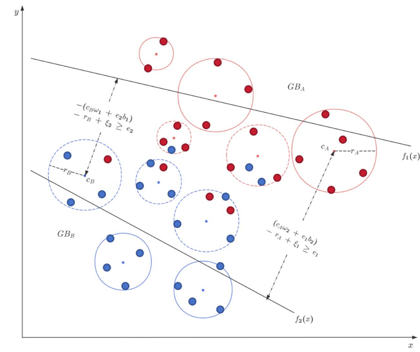

Fig. 4. GBFTSVM classifier.

B. Linear Granular-Ball Fuzzy Twin Support Vector Machine Classifier

Consider a family of granular-balls $\mathcal{GB} = \{(c_i, r_i, p_i, y_i) \mid 1 \leq i \leq m\}$, where c_i is the center of granular-ball GB_i, r_i is the radius of granular-ball GB_i, p_i is its purity, and $y_i \in \{-1, +1\}$ indicates its class label. The linear GBFTSVM classifier constructs two nonparallel hyperplanes by solving the following QPPs:

$$\begin{aligned} \min_{\omega_1, b_1, \xi_2} \quad & \frac{1}{2}(c_A\omega_1 + e_1b_1)^T(c_A\omega_1 + e_1b_1) + C_1 s_B^T \xi_2, \\ \text{s.t.} \quad & -(c_B\omega_1 + e_2b_1) - r_B + \xi_2 \geq e_2, \xi_2 \geq 0 \end{aligned} \tag{29}$$

and

$$\begin{aligned} \min_{\omega_2, b_2, \xi_1} \quad & \frac{1}{2}(c_B\omega_2 + e_2b_2)^T(c_B\omega_2 + e_2b_2) + C_2 s_A^T \xi_1, \\ \text{s.t.} \quad & (c_A\omega_2 + e_1b_2) - r_A + \xi_1 \geq e_1, \xi_1 \geq 0 \end{aligned} \tag{30}$$

where C_1 and C_2 are constants and both are greater than 0, and e_1 and e_2 are unit vectors of the appropriate dimension, $s_A \in \mathcal{R}$ and $s_B \in \mathcal{R}$ are the score values of positive and negative granular-balls, respectively.

We tackle the QPP of the linear GBFTSVM classifier by incorporating Lagrange multipliers $\alpha_1,\ \beta_1,\ \alpha_2$, and β_2 as follows:

$$\begin{aligned} & L(\omega_1, b_1, \xi_2, \alpha_1, \beta_1) \\ & \quad = \frac{1}{2}\|c_A\omega_1 + e_1b_1\|^2 + C_1 s_B^T \xi_2 - \alpha_1^T(-(c_B\omega_1 + e_2b_1) \\ & \qquad + \xi_2 - r_B - e_2) - \beta_1^T \xi_2 \end{aligned} \tag{31}$$

where α_1 and β_1 are Lagrangian multipliers.

According to KKT conditions, we get

$$\frac{\partial L}{\partial \omega_1} = c_A^T(c_A\omega_1 + e_1b_1) + c_B^T\alpha = 0; \tag{32}$$

$$\frac{\partial L}{\partial b_1} = e_1^T(c_A\omega_1 + e_1b_1) + e_2^T\alpha = 0; \tag{33}$$

$$\frac{\partial L}{\partial \xi_2} = C_1 s_B^T - \alpha_1 - \beta_1 = 0. \tag{34}$$

From (32) and (33), we obtain

$$\begin{bmatrix} c_A^T \\ e_1^T \end{bmatrix} \begin{bmatrix} c_A & e_1 \end{bmatrix} \begin{bmatrix} \omega_1 \\ b_1 \end{bmatrix} + \begin{bmatrix} c_B^T \\ e_2^T \end{bmatrix} \alpha_1 = 0. \tag{35}$$

Simplifying, we write

$$E^T E u + F^T \alpha = 0 \tag{36}$$

where $E = [c_A \quad e_1]$, $F = [c_B \quad e_2]$, and $u = [\omega_1 \quad b_1]^T$. By adding the regularization item, we obtain

$$u = -(E^T E + \varepsilon I)^{-1} F^T \alpha_1. \tag{37}$$

Similarly, for the second hyperplane, we write

$$v = (S^T S + \varepsilon I)^{-1} R^T \alpha_2 \tag{38}$$

where $R = [c_A \quad e_1]$, $S = [c_B \quad e_2]$, and $v = [\omega_2 \quad b_2]^T$.

The dual optimization problems for the two hyperplanes are formulated as

$$\begin{aligned} \max_{\alpha_1} \quad & \alpha_1^T (e_2 + r_B) - \frac{1}{2} \alpha_1^T F (E^T E)^{-1} F^T \alpha_1, \\ \text{s.t.} \quad & 0 \leq \alpha_1 \leq C_3 s_B \end{aligned} \tag{39}$$

and

$$\begin{aligned} \max_{\alpha_2} \quad & \alpha_2^T (e_1 + r_A) - \frac{1}{2} \alpha_2^T R (S^T S)^{-1} R^T \alpha_2, \\ \text{s.t.} \quad & 0 \leq \alpha_2 \leq C_4 s_A. \end{aligned} \tag{40}$$

For a new input data $x \,\epsilon\, \mathcal{R}^d$, the predicted class $t \in \{1, 2\}$ is determined by the hyperplane closer to the input

$$\text{Class}\, t = arg \underset{t \in \{1,2\}}{min} \frac{|\langle \omega_t, x \rangle + b_t|}{\|\omega_t\|}. \tag{41}$$

The process of constructing the GBFTSVM classifier is summarized in Algorithm 2. It involves computing granular-ball scores, building optimization problems, and solving them iteratively to obtain the hyperplane parameters.

Assume n samples generate m granular-balls ($m < n$), with each class containing approximately $m/2$ granular-balls, the time complexity of GBFTSVM is $O(2 \times (m/2)^3)$. If the number of generated granular-balls m is approximately $n/2$, the computational speed of GBFTSVM is eight times faster than TWSVM.

Algorithm 2: GBFTSVM Classifier.

Input: Granular-balls $\mathcal{GB} = \{(c_i, r_i, p_i, y_i) \mid i = 1, 2, \ldots, m\}$.
Output: Hyperplane parameters ω_1, ω_2, b_1, and b_2.

Use (25) and (27) to calculate μ_{GB_i} and θ_{GB_i};
Initialize s_i as empty matrices;
for each $GB_i \in \mathcal{GB}$ **do**
  if $p_i = 1$ **then**
    add μ_{GB_i} to matrix s_i;
  else
    add θ_{GB_i} to matrix s_i;
  end if
end for
Initialize c_A, c_B, r_A, r_B, s_A, and s_B as empty matrices;
for each $GB_i \in \mathcal{GB}$ **do**
  if $y_i = 1$ **then**
    add c_i, r_i, and s_i to matrices c_A, r_A, and s_A, respectively;
  else
    add c_i, r_i, and s_i to matrices c_B, r_B, and s_B, respectively;
  end if
end for
Use (39) and (40) to define the objective function;
Perform L-BFGS-B optimization for α_1 and α_2;
Use (37) to calculate ω_1 and b_1;
Use (38) to calculate ω_2 and b_2;
return Hyperplane parameters ω_1, ω_2, b_1, and b_2.

V. Experimental Analysis

In this section, we present a comparative analysis of GBFTSVM and GBTWSVM against seven established methods, including TWSVM [6], EFSVM [16], IFTSVM [17], GBKNN [34], GBFSVM [35], GBSVM [38], and 3WC-GBNRS++ [40]. All methods were implemented in Python 3.11 and executed on a desktop computer equipped with an Intel Core i7-10700 CPU operating at 2.90 GHz, with 16 GB of RAM.

A. Experimental Datasets

We utilize 21 benchmark datasets obtained from the UCI Machine Learning Repository [60]. The statistical characteristics are summarized in Table I. To assess the performance of the nine methods, we employ four evaluation metrics: Running time, Accuracy (Acc), Precision (Prec), and Recall (Rec). Each dataset is partitioned into training and testing subsets using an $8:2$ ratio. In the experiments, to ensure consistency across all tests, we adopted the classical k-means-based granular-ball generation method, where the radius r_i of each granular-ball GB_i is calculated as the average distance of all data points within the granular-ball. For every experiment conducted on a dataset, we systematically optimize the purity threshold in increments of 0.01. The highest classification accuracy obtained across various purity thresholds is selected as the final accuracy for that dataset. The value of the small positive constant ε in (25) was set to 0.00001. To ensure the reliability of the results, each experiment is repeated ten times, and the average value across these repetitions is reported as the final evaluation outcome.

B. Penalty Parameters

We conduct a grid search over the penalty parameters used in different methods, and report the best-performing results as the final outcomes. The parameter settings for the TWSVM,

TABLE I
TWENTY-ONE DATASETS FOR EXPERIMENT

Datasets	Numbers of samples	Numbers of attributes
Australian	690	13
Breast-cancer	277	9
Breast-cancer-wisc	683	9
Chronic-kidney-disease	158	24
Congressional-voting-records	231	16
Conn-bench-sonar-mines-rocks	208	60
Credit-approval	653	15
Diabetes	768	7
Diabetes-upload	520	16
Electrical	10000	13
Fourclass	682	2
German.numer	1000	23
Heart	270	12
Ionosphere	351	34
Liver-disorders	145	4
Messidor-features	1151	19
Spambase	4601	57
Tic-tac-toe	958	8
Twonorm	7400	20
WDBC	569	30
Wholesale-customers	440	7

IFTSVM, GBTWSVM, and GBFTSVM classifiers are listed as follows: $C_i\,(i=1,2,3,4)$ is systematically explored over the grid $\{2^i \mid i=-5,-4,\ldots,+4,+5\}$, with the constraints $C_1=C_3$, $C_2=C_4$. For the EFSVM, GBSVM, and GBFSVM classifiers, the parameter C is similarly optimized over the grid $\{2^i \mid i=-5,-4,\ldots,+4,+5\}$. We select the parameter settings that yield the highest accuracy by each of the nine models on the datasets as the final configurations. In addition, we present the optimized parameters for these methods across different datasets in Table II.

C. Experimental Results on Datasets Without Noise

1) Comparison of Training Times: In the absence of noise, the training times for the evaluated models across various datasets are presented in Table III. Notably, while the 3WC-GBNRS++ classifier achieves the shortest training time on most datasets, GBTWSVM and GBFTSVM exhibit significant speed advantages as dataset size increases. For instance, on the Electrical dataset, GBTWSVM's training speed is ten times faster than that of 3WC-GBNRS++. In addition, in terms of average training time and average ranking across all datasets, GBTWSVM emerges as the fastest, followed by GBFTSVM. While 3WC-GBNRS++ ranks slightly higher overall, its efficiency on larger datasets lags behind GBTWSVM. These findings underscore GBTWSVM's distinct advantage in terms of both overall performance and scalability for large datasets. Two primary factors contribute to these observations: First, the number of granular-balls generated in the datasets is significantly smaller than the sample size. Second, both GBTWSVM and GBFTSVM derive the hyperplane by two smaller-scale QPPs instead of a single large-scale one, thereby reducing computational complexity. While the GBTWSVM classifier achieves slightly worse accuracy than the GBFTSVM classifier, it exhibits faster. This efficiency arises because GBFTSVM requires the calculation of a scoring function for each granular ball to evaluate its contribution to classification, whereas GBTWSVM does not include this step.

2) Comparison of Accuracy, Precision, and Recall: To comprehensively evaluate the performance of the GBTWSVM and GBFTSVM classifiers on multiple datasets without noise, we conduct a rigorous comparison of nine models across 21 benchmark datasets. These models are evaluated based on their accuracy, precision, and recall for classification. The results of this evaluation are summarized in Table IV and illustrated in Figs. S1, S2, and S3 (see supplementary materials). After a thorough analysis, we arrive at the following conclusions: The GBFTSVM classifier exhibits the highest accuracy, precision, and recall across 16 of the 21 datasets, and firmly establishes its superior classification capabilities. Notably, the GBFTSVM classifier exhibits a relatively low standard deviation in accuracy, indicating its consistent and reliable performance across datasets. While the GBTWSVM classifier trails the GBFTSVM classifier slightly in terms of overall accuracy, it still achieves high accuracy on eleven datasets with a low standard deviation, positioning it as a strong contender among the remaining eight models. Furthermore, we compare the average accuracy of each model across all datasets. Evidently, the GBFTSVM classifier achieves the highest average accuracy, and outperforms the other models by 1% –30% , which underscores its superior classification performance. In comparison with the GBTWSVM classifier, the notable improvement of the GBFTSVM classifier's average accuracy validates the significance of our optimizations and enhancements to the membership function for classification.

To overcome the potential bias caused by a model's high accuracy in one dataset and low accuracies in others, we calculate the average rank of each model across all datasets. The model with the highest accuracy is ranked first, and in cases of equal accuracy, the average of the corresponding ranks is used. The GBFTSVM classifier emerges with the lowest average rank, and firmly establishes its superiority among all the compared models. Similarly, the GBTWSVM classifier, with the second-lowest average rank, demonstrates strong performance relative to the other models, apart from the GBFTSVM classifier.

D. Experimental Results on Datasets With Noise

To assess the robustness of the GBTWSVM classifier and the GBFTSVM classifier to noise, we generated noisy datasets by randomly flipping the labels of 5% and 10% of the samples to 21 datasets and compare the classification accuracy of nine models. The results are shown in Table V, and illustrated in Fig. S4 (see supplementary materials). Due to the extended training time of GBSVM, which exceeded seven days to complete a single experiment under both the 5% and 10% noise conditions, and the requirement to run the experiment ten times, its results are excluded from the analysis. From the results in Table V, the GBFTSVM classifier achieves the highest accuracy on 16 datasets with 5% noise and on 19 datasets with 10% noise,

TABLE II
OPTIMAL PARAMETERS OF SEVEN MODELS ON UCI DATASETS WITHOUT NOISE

Dataset	TWSVM C_1, C_2	EFSVM C	IFTSVM C_1, C_2	GBSVM C	GBFSVM C	GBTWSVM C_1, C_2	GBFTSVM C_1, C_2
Australian	2^2, 2^0	2^{-5}	2^2, 2^{-4}	2^0	2^0	2^{-4}, 2^{-4}	2^{-3}, 2^{-5}
Breast-cancer	2^{-5}, 2^{-4}	2^{-5}	2^{-5}, 2^{-5}	2^0	2^{-1}	2^{-5}, 2^{-3}	2^4, 2^{-2}
Breast-cancer-wisc	2^{-5}, 2^{-1}	2^{-4}	2^{-2}, 2^2	2^{-2}	2^0	2^0, 2^{-4}	2^2, 2^{-2}
Chronic-kidney-disease	2^{-5}, 2^{-5}	2^{-5}	2^{-5}, 2^{-5}	2^0	2^{-1}	2^{-4}, 2^{-5}	2^{-1}, 2^0
Congressional-voting-records	2^{-5}, 2^{-5}	2^{-5}	2^{-5}, 2^{-5}	2^1	2^{-1}	2^{-4}, 2^0	2^{-3}, 2^{-1}
Conn-bench-sonar-mines-rocks	2^0, 2^{-5}	2^5	2^{-4}, 2^0	2^{-5}	2^0	2^0, 2^{-1}	2^3, 2^2
Credit-approval	2^{-2}, 2^{-5}	2^{-5}	2^2, 2^{-4}	2^{-4}	2^0	2^1, 2^0	2^0, 2^3
Diabetes	2^{-5}, 2^{-4}	2^{-5}	2^4, 2^{-1}	2^0	2^{-1}	2^3, 2^{-1}	2^{-4}, 2^{-5}
Diabetes-upload	2^0, 2^0	2^{-3}	2^{-3}, 2^{-3}	2^0	2^0	2^{-2}, 2^{-3}	2^2, 2^2
Electrical	2^{-4}, 2^{-3}	2^3	2^{-1}, 2^{-1}	2^0	2^0	2^2, 2^1	2^3, 2^4
Fourclass	2^0, 2^{-1}	2^3	2^1, 2^3	2^0	2^{-1}	2^2, 2^0	2^{-5}, 2^{-4}
German.numer	2^{-5}, 2^{-4}	2^{-5}	2^{-1}, 2^5	2^{-3}	2^{-1}	2^2, 2^3	2^{-1}, 2^{-1}
Heart	2^{-4}, 2^{-3}	2^{-1}	2^2, 2^2	2^1	2^0	2^{-3}, 2^{-5}	2^1, 2^{-5}
Ionosphere	2^{-4}, 2^{-5}	2^{-5}	2^{-5}, 2^{-5}	2^{-4}	2^0	2^{-5}, 2^3	2^{-4}, 2^0
Liver-disorders	2^{-5}, 2^{-2}	2^{-1}	2^{-4}, 2^{-5}	2^{-4}	2^{-1}	2^{-1}, 2^{-4}	2^1, 2^{-4}
Messidor-features	2^{-3}, 2^{-5}	2^5	2^0, 2^{-4}	2^3	2^0	2^3, 2^4	2^{-3}, 2^{-3}
Spambase	2^{-5}, 2^{-5}	2^5	2^2, 2^{-2}	2^1	2^0	2^{-2}, 2^{-2}	2^1, 2^{-2}
Tic-tac-toe	2^{-5}, 2^{-5}	2^{-5}	2^4, 2^0	2^2	2^{-1}	2^1, 2^0	2^{-2}, 2^{-2}
Twonorm	2^2, 2^2	2^1	2^{-3}, 2^{-5}	2^0	2^0	2^{-4}, 2^{-2}	2^{-5}, 2^{-5}
WDBC	2^4, 2^3	2^0	2^{-4}, 2^{-4}	2^3	2^{-1}	2^{-5}, 2^1	2^0, 2^2
Wholesale-customers	2^3, 2^1	2^{-5}	2^{-3}, 2^{-1}	2^1	2^0	2^{-5}, 2^{-4}	2^{-2}, 2^{-2}

TABLE III
RUNNING TIME OF NINE MODELS ON UCI DATASETS WITHOUT NOISE

Dataset	TWSVM	EFSVM	IFTSVM	GBSVM	GBFSVM	GBKNN	3WC-GBNRS++	GBTWSVM	GBFTSVM
Australian	2.309	4.178	5.640	2.659	6.764	11.641	**0.070**	0.172	0.490
Breast-cancer	0.289	0.162	1.495	0.948	0.638	3.056	**0.010**	0.067	0.100
Breast-cancer-wisc	2.269	4.541	5.431	0.134	0.032	0.634	**0.012**	0.016	0.054
Chronic-kidney-disease	0.450	0.055	1.061	0.004	0.046	1.350	0.004	**0.003**	0.009
Congressional-voting-records	0.762	0.109	1.703	0.224	0.130	0.865	**0.005**	0.017	0.037
Conn-bench-sonar-mines-rocks	0.862	0.102	0.451	0.639	0.868	1.895	**0.006**	0.032	0.064
Credit-approval	2.099	3.475	5.195	2.081	6.884	10.730	**0.071**	0.090	0.171
Diabetes	0.762	5.443	4.202	21.807	4.382	11.702	**0.084**	0.194	0.274
Diabetes-upload	1.541	1.687	4.215	1.481	0.136	2.710	**0.008**	0.045	0.110
Electrical	536.677	1511.619	2055.804	368816.628	347.615	668.800	31.913	**3.126**	3.662
Fourclass	1.233	7.462	7.034	0.062	0.057	1.125	**0.024**	0.034	0.088
German.numer	1.555	13.508	6.120	273.837	22.802	18.630	**0.152**	1.038	1.147
Heart	1.327	0.144	1.565	0.821	0.786	3.837	**0.020**	0.064	0.122
Ionosphere	1.465	0.266	2.963	4.613	0.275	1.992	**0.011**	0.075	0.118
Liver-disorders	0.120	0.022	0.137	0.225	0.154	1.872	**0.005**	0.027	0.050
Messidor-features	2.120	22.039	6.854	1021.768	42.537	23.772	**0.322**	0.940	1.671
Spambase	99.972	91.115	651.741	4017.286	201.019	135.878	3.537	**3.129**	3.176
Tic-tac-toe	0.730	11.010	4.421	322.375	27.621	16.662	**0.235**	0.692	1.023
Twonorm	201.740	1558.699	2574.803	1618.394	69.135	4.726	4.095	4.323	**2.384**
WDBC	1.649	2.309	4.709	0.417	0.448	1.998	**0.025**	0.040	0.112
Wholesale-customers	1.499	1.046	3.284	0.993	0.356	2.699	**0.021**	0.107	0.112
Average Time	41.020	154.238	254.706	17909.876	34.890	44.123	1.935	0.678	0.713
Average Rank	5.571	5.762	7.381	6.571	5.810	7.524	1.333	1.952	3.095

outperforming the other eight models. Notably, on the Messidor-features, Diabetes-upload, and WDBC datasets, the GBFTSVM classifier, although not the top performer in noise-free conditions, demonstrates improved stability under noise, leading to better classification accuracy, particularly with 10% label noise. It is noteworthy that classifiers based on granular-balls exhibits a relatively stable accuracy fluctuation of approximately 2% with noise addition, compared to a fluctuation of over 2% for classifiers based on point inputs. This suggests that classifiers based on granular-balls offer better robustness to noise, maintaining prediction stability more effectively. Furthermore, the GBFTSVM classifier emerges as the top performer in terms of average accuracy across all noise levels (5% and 10%). This can be attributed to several factors: First, the coarser granularity of the granular-balls and the assignment of majority labels to noisy points mitigate the impact of label noise. Second, the GBFTSVM classifier employs two symmetric support vectors based on granular-balls, which, through their symmetry, effectively resists

TABLE IV
ACCURACY, PRECISION, AND RECALL OF NINE MODELS ON UCI DATASETS WITHOUT NOISE

Dataset	TWSVM Acc±Sd (Prec,Rec)	EFSVM Acc±Sd (Prec,Rec)	IFTSVM Acc±Sd (Prec,Rec)	GBSVM Acc±Sd (Prec,Rec)	GBFSVM Acc±Sd (Prec,Rec)	GBKNN Acc±Sd (Prec,Rec)	3WC-GBNRS++ Acc±Sd (Prec,Rec)	GBTWSVM Acc±Sd (Prec,Rec)	GBFTSVM Acc±Sd (Prec,Rec)
Australian	0.90±0.03 (0.90,0.90)	0.84±0.08 (0.83,0.84)	0.90±0.01 (0.90,0.90)	0.86±0.02 (0.89,0.82)	0.84±0.04 (0.85,0.84)	0.67±0.02 (0.62,0.58)	0.84±0.01 (0.84,0.82)	0.91±0.03 (0.91,0.91)	**0.92±0.02** **(0.92,0.92)**
Breast-cancer	0.84±0.05 (0.83,0.84)	0.84±0.05 (0.76,0.84)	0.86±0.06 (0.85,0.86)	0.82±0.05 (0.15,0.53)	0.87±0.09 (0.88,0.87)	0.70±0.06 (0.33,0.22)	0.59±0.01 (0.15,0.15)	0.91±0.04 (0.91,0.91)	**0.92±0.03** **(0.93,0.92)**
Breast-cancer-wisc	0.99±0.01 (0.99,0.99)	0.98±0.02 (0.98,0.98)	0.99±0.01 (0.99,0.99)	0.94±0.03 (0.91,0.93)	0.98±0.02 (0.98,0.98)	0.95±0.02 (0.93,0.97)	0.96±0.00 (0.99,0.96)	0.98±0.02 (0.98,0.98)	**0.99±0.01** **(0.99,0.99)**
Chronic-kidney-disease	1.00±0.00 (1.00,1.00)	0.99±0.03 (0.99,0.99)	1.00±0.00 (1.00,1.00)	0.87±0.12 (0.56,0.80)	0.96±0.21 (0.96,0.96)	0.80±0.06 (0.75,0.42)	0.88±0.01 (0.90,0.76)	0.98±0.03 (0.98,0.98)	**1.00±0.00** **(1.00,1.00)**
Congressional-voting-records	0.98±0.02 (0.98,0.98)	0.98±0.03 (0.98,0.98)	0.99±0.02 (0.99,0.99)	0.93±0.04 (0.96,0.90)	0.92±0.05 (0.92,0.92)	0.88±0.05 (0.90,0.84)	0.60±0.02 (0.40,0.40)	0.97±0.04 (0.97,0.97)	**0.99±0.02** **(0.99,0.99)**
Conn-bench-sonar-mines-rocks	0.85±0.04 (0.86,0.85)	0.80±0.08 (0.82,0.80)	0.79±0.05 (0.80,0.79)	0.77±0.06 (0.77,0.71)	0.71±0.10 (0.77,0.71)	0.81±0.08 (0.81,0.77)	0.90±0.01 (0.90,0.90)	0.93±0.03 (0.94,0.93)	**0.97±0.04** **(0.97,0.97)**
Credit-approval	0.91±0.03 (0.92,0.91)	0.82±0.11 (0.79,0.82)	0.89±0.02 (0.89,0.89)	0.85±0.05 (0.87,0.81)	0.88±0.05 (0.89,0.88)	0.67±0.03 (0.66,0.58)	0.80±0.01 (0.68,0.69)	0.89±0.02 (0.90,0.89)	**0.92±0.03** **(0.92,0.92)**
Diabetes	0.81±0.03 (0.82,0.81)	0.65±0.16 (0.71,0.65)	0.76±0.02 (0.76,0.76)	0.79±0.03 (0.88,0.81)	0.76±0.05 (0.78,0.76)	0.72±0.02 (0.77,0.82)	0.73±0.02 (0.81,0.76)	0.83±0.02 (0.83,0.83)	**0.84±0.03** **(0.85,0.84)**
Diabetes-upload	0.96±0.03 (0.96,0.96)	0.92±0.03 (0.93,0.92)	0.94±0.04 (0.94,0.94)	0.77±0.02 (0.98,0.75)	0.82±0.08 (0.83,0.82)	0.74±0.05 (0.80,0.84)	**1.00±0.01** **(1.00,1.00)**	0.96±0.02 (0.96,0.96)	0.98±0.02 (0.98,0.98)
Electrical	0.99±0.00 (0.99,0.99)	**1.00±0.00** **(1.00,1.00)**	0.98±0.01 (0.98,0.98)	0.99±0.02 (1.00,0.96)	0.80±0.07 (0.82,0.80)	0.77±0.01 (0.72,0.63)	0.97±0.02 (0.96,0.89)	**1.00±0.00** **(1.00,1.00)**	**1.00±0.00** **(1.00,1.00)**
Fourclass	0.79±0.04 (0.81,0.79)	0.74±0.06 (0.81,0.74)	0.82±0.03 (0.83,0.82)	0.71±0.06 (0.25,0.75)	0.76±0.04 (0.78,0.76)	**0.99±0.00** **(0.99,0.99)**	0.90±0.01 (0.70,0.70)	0.83±0.03 (0.85,0.83)	0.84±0.03 (0.85,0.84)
German.numer	0.77±0.03 (0.77,0.77)	0.75±0.05 (0.71,0.75)	0.76±0.03 (0.76,0.76)	0.79±0.03 (0.69,0.64)	0.80±0.04 (0.82,0.80)	0.69±0.02 (0.46,0.26)	0.81±0.02 (0.20,0.12)	0.81±0.04 (0.80,0.81)	**0.83±0.03** **(0.82,0.83)**
Heart	0.88±0.06 (0.89,0.88)	0.89±0.06 (0.90,0.89)	0.90±0.04 (0.90,0.90)	0.82±0.02 (0.80,0.82)	0.83±0.08 (0.85,0.83)	0.60±0.05 (0.57,0.49)	0.83±0.01 (0.67,0.77)	0.91±0.05 (0.91,0.91)	**0.95±0.04** **(0.95,0.95)**
Ionosphere	0.93±0.04 (0.93,0.93)	0.86±0.14 (0.84,0.86)	0.95±0.03 (0.95,0.95)	0.88±0.05 (0.92,0.91)	0.78±0.06 (0.74,0.78)	0.65±0.06 (0.99,0.44)	0.43±0.02 (0.28,0.90)	0.93±0.02 (0.94,0.93)	**0.97±0.02** **(0.97,0.97)**
Liver-disorders	0.87±0.12 (0.86,0.87)	0.75±0.07 (0.82,0.75)	0.85±0.08 (0.87,0.85)	0.77±0.04 (0.57,0.86)	0.79±0.10 (0.78,0.79)	0.65±0.05 (0.55,0.38)	0.52±0.01 (0.85,0.43)	0.90±0.05 (0.91,0.90)	**0.93±0.04** **(0.94,0.93)**
Messidor-features	0.80±0.03 (0.82,0.80)	0.70±0.05 (0.76,0.70)	0.76±0.02 (0.78,0.76)	0.73±0.04 (0.58,0.82)	0.71±0.04 (0.71,0.71)	0.65±0.02 (0.67,0.67)	0.54±0.01 (0.91,0.56)	**0.82±0.03** **(0.82,0.82)**	0.80±0.03 (0.82,0.80)
Spambase	0.85±0.02 (0.87,0.85)	0.91±0.04 (0.91,0.91)	0.88±0.02 (0.89,0.88)	0.48±0.26 (0.00,0.01)	0.60±0.13 (0.60,0.60)	0.80±0.01 (0.78,0.70)	0.84±0.00 (0.63,0.81)	**0.94±0.01** **(0.94,0.94)**	0.93±0.00 (0.93,0.93)
Tic-tac-toe	0.70±0.04 (0.68,0.70)	0.56±0.13 (0.33,0.56)	0.70±0.04 (0.73,0.70)	0.67±0.02 (0.79,0.73)	0.68±0.04 (0.55,0.68)	0.75±0.03 (0.78,0.87)	0.75±0.01 (1.00,0.75)	0.75±0.05 (0.76,0.75)	**0.77±0.03** **(0.80,0.77)**
Twonorm	0.98±0.00 (0.98,0.98)	0.98±0.01 (0.98,0.98)	0.98±0.01 (0.98,0.98)	0.96±0.00 (0.96,0.96)	0.97±0.00 (0.97,0.97)	0.98±0.00 (0.97,0.98)	0.98±0.01 (0.98,0.98)	0.98±0.00 (0.98,0.98)	**0.98±0.00** **(0.98,0.98)**
WDBC	0.98±0.01 (0.98,0.98)	0.97±0.02 (0.98,0.97)	1.00±0.01 (1.00,1.00)	0.97±0.01 (0.99,0.97)	0.87±0.15 (0.85,0.87)	0.91±0.02 (0.92,0.95)	**1.00±0.00** **(0.89,0.90)**	0.96±0.03 (0.97,0.96)	0.99±0.01 (0.99,0.99)
Wholesale-customers	0.95±0.04 (0.95,0.95)	0.85±0.21 (0.84,0.85)	0.94±0.03 (0.94,0.94)	0.85±0.07 (0.95,0.86)	0.84±0.04 (0.85,0.84)	0.89±0.01 (0.93,0.91)	0.78±0.01 (0.68,0.70)	0.95±0.04 (0.95,0.95)	**0.96±0.02** **(0.97,0.96)**
Average Accuracy	0.89	0.85	0.89	0.82	0.82	0.77	0.79	0.91	**0.93**
Average Rank	3.93	6.07	4.10	6.88	6.48	7.19	6.00	2.88	1.48

noise and outliers, thereby enhancing the model's generalization ability. Third, the assignment of scoring functions to granular-balls helps distinguish supportive granular-balls, minimizing their detrimental effect on the separation hyperplane, and further improving the classifier's robustness to noise.

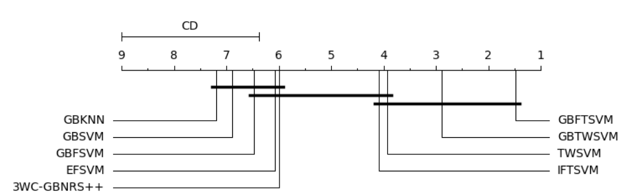

Fig. 5. Comparison of nine models in terms of CD diagrams.

E. Statistical Analysis

To validate the statistical significance of the GBFTSVM classifier, we perform the Friedman test followed by the Nemenyi post-hoc test across nine models on 21 datasets without noise. Initially, we assume that all models are equivalent under the null hypothesis. The Friedman statistic follows a chi-square distribution, and is calculated using the formula: $\chi_F^2 = \frac{12N}{M(M+1)}[\sum_{j=1}^{M} R_j^2 - \frac{M(M+1)^2}{4}]$, where R_j $(j = 1, 2, \ldots 7)$ stands for the average rank of the jth model, N is the number of datasets, and M is the number of models. Alternatively, the Friedman statistic follows an F-distribution with $((M-1), (M-1)(N-1))$ degrees of freedom, and is computed as: $F_F = \frac{(N-1)\chi_F^2}{N(M-1)-\chi_F^2}$. From Table IV, we obtain an F_F value of 22.16 with degrees of freedom (8160). At a significance level of 0.05, the critical value of $F(8160)$ is 1.9967. Since F_F exceeds this critical value, we reject the null hypothesis. Subsequently, we ultilize the Nemenyi post-hoc test to further distinguish these models. It involves calculating the critical difference (CD): $\text{CD} = q_\alpha\sqrt{\frac{M(M+1)}{6N}}$. At a significance level of 0.05, q_α is 2.949. To visualize the differences among nine classifiers, we generate a CD diagram depicted in Fig. 5.

TABLE V
ACCURACY OF NINE MODELS ON UCI DATASETS WITH DIFFERENT NOISE LEVELS

Dataset	Noise Level	TWSVM	EFSVM	IFTSVM	GBSVM	GBFSVM	GBKNN	3WC-GBNRS++	GBTWSVM	GBFTSVM
Australian	0.05	0.88	0.82	0.89	0.87	0.84	0.67	0.79	0.90	**0.90**
	0.1	0.88	0.88	0.89	0.87	0.86	0.70	0.70	0.89	**0.91**
Breast-cancer	0.05	0.80	0.79	0.84	0.82	0.82	0.76	0.39	**0.90**	**0.90**
	0.1	0.81	0.83	0.86	0.79	0.88	0.81	0.32	0.88	**0.90**
Breast-cancer-wisc	0.05	0.98	0.95	0.98	0.83	0.98	0.85	0.89	0.99	**0.99**
	0.1	0.98	0.93	0.97	0.90	0.98	0.76	0.72	0.99	**0.99**
Chronic-kidney-disease	0.05	0.99	**1.00**	**1.00**	0.99	**1.00**	0.84	0.82	0.99	**1.00**
	0.1	0.99	**1.00**	**1.00**	0.98	0.99	0.87	0.73	**1.00**	0.99
Congressional-voting-records	0.05	**0.98**	0.97	**0.98**	0.91	0.90	0.75	0.50	0.98	**0.98**
	0.1	0.97	0.95	0.98	0.92	0.93	0.78	0.20	0.98	**0.99**
Conn-bench-sonar-mines-rocks	0.05	0.83	0.83	0.79	0.81	0.60	0.67	0.90	0.90	**0.92**
	0.1	0.80	0.75	0.76	0.78	0.61	0.74	0.75	0.90	**0.90**
Credit-approval	0.05	0.90	0.77	0.88	0.86	0.88	0.64	0.88	0.89	**0.90**
	0.1	0.89	0.87	0.89	0.89	0.87	0.70	0.67	0.90	**0.92**
Diabetes	0.05	0.81	0.62	0.80	0.77	0.75	0.64	0.60	0.84	**0.85**
	0.1	0.79	0.47	0.76	0.79	0.74	0.65	0.63	0.83	**0.84**
Diabetes-upload	0.05	0.94	0.83	0.94	0.90	0.90	0.61	**0.98**	0.96	0.96
	0.1	0.93	0.86	0.93	0.83	0.82	0.65	0.73	0.97	**0.97**
Electrical	0.05	0.93	0.97	0.96	*	0.81	0.76	0.91	**1.00**	**1.00**
	0.1	0.89	0.90	0.93	*	0.80	0.80	0.87	**0.99**	0.99
Fourclass	0.05	0.80	0.77	0.78	0.65	0.73	**0.89**	0.43	0.82	0.83
	0.1	0.79	0.71	0.79	0.75	0.73	**0.84**	0.29	0.82	0.82
German.numer	0.05	0.78	0.79	0.78	0.77	0.78	0.76	0.60	0.82	**0.83**
	0.1	0.77	0.76	0.76	0.77	0.78	0.82	0.68	0.80	**0.82**
Heart	0.05	0.88	0.81	0.86	0.89	0.86	0.66	0.71	0.91	**0.92**
	0.1	0.86	0.81	0.87	0.83	0.81	0.69	0.72	0.91	**0.93**
Ionosphere	0.05	0.93	0.76	**0.94**	0.83	0.81	0.62	0.57	0.93	**0.94**
	0.1	0.91	0.71	0.94	0.88	0.78	0.68	0.60	0.93	**0.96**
Liver-disorders	0.05	0.83	0.83	0.83	0.77	0.73	0.69	0.44	0.90	**0.94**
	0.1	0.81	0.75	0.81	0.71	0.59	0.78	0.54	0.88	**0.93**
Messidor-features	0.05	0.78	0.69	0.75	0.55	0.70	0.64	0.49	**0.80**	0.79
	0.1	0.76	0.67	0.73	0.68	0.71	0.68	0.52	0.77	**0.78**
Spambase	0.05	0.83	0.88	0.86	0.32	0.62	0.75	0.74	0.93	**0.94**
	0.1	0.80	0.86	0.84	0.28	0.61	0.78	0.50	0.92	**0.94**
Tic-tac-toe	0.05	0.68	0.46	0.68	0.71	0.67	0.61	0.75	0.74	**0.75**
	0.1	0.67	0.61	0.63	0.68	0.63	0.66	0.67	0.73	**0.73**
Twonorm	0.05	0.98	0.98	0.96	0.96	0.98	0.85	0.93	**0.98**	0.98
	0.1	0.98	0.91	0.96	0.97	0.98	0.80	0.87	0.98	**0.98**
WDBC	0.05	0.97	0.97	**0.99**	0.96	0.81	0.77	0.88	0.97	0.98
	0.1	0.97	0.90	**0.98**	0.93	0.89	0.70	0.72	0.97	**0.98**
Wholesale-customers	0.05	0.93	0.82	0.94	0.88	0.82	0.74	0.58	0.95	**0.96**
	0.1	0.92	0.64	0.90	0.90	0.82	0.72	0.39	0.95	**0.95**
Average Accuracy	0.05	0.88	0.82	0.88	0.80	0.81	0.72	0.70	0.91	**0.92**
	0.1	0.86	0.80	0.87	0.81	0.80	0.74	0.61	0.90	**0.91**

* Due to the extended training time of GBSVM, which exceeded seven days to complete a single experiment under both the 5% and 10% noise conditions, and the requirement to run the experiment ten times, its results are excluded from the analysis.

This diagram clearly shows that the horizontal line representing the GBFTSVM classifier does not overlap with the lines for the 3WC-GBNRS++, EFSVM, GBFSVM, GBSVM, and GBKNN classifiers. This indicates that the GBFTSVM classifier significantly differs from and outperforms these other models.

VI. CONCLUSION

In this article, inspired by GBC and TWSVM, we have proposed the GBTWSVM classifier for binary classification problems, which utilizes granular-balls as inputs instead of individual samples, and offers a scalable, efficient, and robust data processing method. Subsequently, we have introduced the GBFTSVM classifier by integrating GBC, PFS, and FTSVM, which defines the granular-ball membership and nonmembership functions based on the Pythagorean closeness index. In addition, the GBFTSVM classifier distinguishes the contribution of granular-balls from different regions to classification, further enhancing its effectiveness. Finally, the experimental results conducted on 21 benchmark datasets demonstrate that the GBFTSVM classifier achieves outstanding performance in terms of classification accuracy, precision, recall, and stability, while the GBTWSVM classifier excels in training efficiency.

In real-world applications, there are numerous instances of nonlinear classification problems and multiclass classification challenges. In the future, we will explore methods to integrate granular-ball computing with nonlinear and multiclass tasks to enhance model performance on complex data. We also investigate the combination of granular-ball computing with variant models of twin support vector machines to further improve classification performance. In addition, advanced techniques such as deep learning or reinforcement learning will be introduced to optimize both the generation of granular-balls and the classification processes.

REFERENCES

[1] V. N. Vapnik, *Statistical Learning Theory*, vol. 1. Hoboken, NJ, USA: Wiley, Sep. 1998.

[2] B. Heisele, P. Ho, and T. Poggio, "Face recognition with support vector machines: Global versus component-based approach," in *Proc. 8th IEEE Int. Conf. Comput. Vis.*, Jul. 2001, vol. 2, pp. 688–694.

[3] O. L. Mangasarian and E. W. Wild, "Multisurface proximal support vector machine classification via generalized eigenvalues," *IEEE Trans. Pattern Anal. Mach. Intell.*, vol. 28, no. 1, pp. 69–74, Jan. 2006.

[4] N. Y. Deng, Y. J. Tian, and C. H. Zhang, *Support Vector Machines: Optimization Based Theory, Algorithms, and Extensions*. Boca Raton, FL, USA: CRC Press, Nov. 2012.

[5] V. N. Vapnik and R. Izmailov, "Knowledge transfer in SVM and neural networks," *Ann. Math. Artif. Intell.*, vol. 81, pp. 3–19, Feb. 2017.

[6] J. R. Khemchandani and S. Chandra, "Twin support vector machines for pattern classification," *IEEE Trans. Pattern Anal. Mach. Intell.*, vol. 29, no. 5, pp. 905–910, May 2007.

[7] J. R. Khemchandani and S. Chandra, "Optimal kernel selection in twin support vector machines," *Optim. Lett.*, vol. 3, no. 1, pp. 77–88, Jan. 2009.

[8] Z. Qi, Y. Tian, and Y. Shi, "Robust twin support vector machine for pattern classification," *Pattern Recognit.*, vol. 46, no. 1, pp. 305–316, Jan. 2013.

[9] X. J. Xie and S. L. Sun, "PAC-bayes bounds for twin support vector machines," *Neurocomputing*, vol. 234, pp. 137–143, Apr. 2017.

[10] X. Peng, "A v-twin support vector machine (v-TSVM) classifier and its geometric algorithms," *Inf. Sci.*, vol. 180, pp. 3863–3875, Oct. 2010.

[11] B. B. Gao, "Coordinate descent fuzzy twin support vector machine for classification," in *Proc. IEEE 14th Int. Conf. Mach. Learn. Appl.*, Dec. 2015, pp. 7–12.

[12] C. F. Lin and S. D. Wang, "Fuzzy support vector machines," *IEEE Trans. Neural Netw.*, vol. 13, no. 2, pp. 464–471, Mar. 2002.

[13] X. W. Yang, G. Q. Zhang, J. Lu, and J. Ma, "A kernel fuzzy c-means clustering fuzzy support vector machine algorithm for classification problems with outliers or noises," *IEEE Trans. Fuzzy Syst.*, vol. 19, no. 1, pp. 105–115, Feb. 2011.

[14] Y. T. Xu, "A rough margin-based linear support vector regression," *Statist. Probability Lett.*, vol. 82, no. 3, pp. 528–534, Mar. 2012.

[15] A. Shigeo, "Fuzzy support vector machines for multilabel classification," *Pattern Recognit.*, vol. 48, no. 6, pp. 2110–2117, Jun. 2015.

[16] Q. Fan, Z. Wang, D. D. Li, D. Q. Gao, and H. Y. Zha, "Entropy-based fuzzy support vector machine for imbalanced datasets," *Knowl.-Based Syst.*, vol. 115, pp. 87–99, Jan. 2017.

[17] S. Rezvani, X. Wang, and F. Pourpanah, "Intuitionistic fuzzy twin support vector machines," *IEEE Trans. Fuzzy Syst.*, vol. 27, no. 11, pp. 2140–2151, Nov. 2019.

[18] D. Gupta, B. Richhariya, and P. Borah, "A fuzzy twin support vector machine based on information entropy for class imbalance learning," *Neural Comput. Appl.*, vol. 31, pp. 7153–7164, Nov. 2019.

[19] Z. Z. Liang and L. Zhang, "Intuitionistic fuzzy twin support vector machines with the insensitive pinball loss," *Appl. Soft Comput.*, vol. 115, Jan. 2022, Art. no. 108231.

[20] H. Duan, T. Feng, S. N. Liu, Y. L. Zhang, and J. L. Su, "Tumor classification of gene expression data by fuzzy hybrid twin SVM," *Chin. J. Electron.*, vol. 31, no. 1, pp. 99–106, Jan. 2022.

[21] Z. Z. Liang and S. F. Ding, "Fuzzy twin support vector machines with distribution inputs," *IEEE Trans. Fuzzy Syst.*, vol. 32, no. 1, pp. 240–254, Jan. 2024.

[22] L. A. Zadeh, "Fuzzy sets and information granularity," *Adv. Fuzzy Set Theory Appl, North Holland, Amsterdam*, pp. 3–18, Jul. 1979.

[23] Y. Y. Yao, "Interpreting concept learning in cognitive informatics and granular computing," *IEEE Trans. Syst., Man, Cybern.*, vol. 39, no. 4, pp. 855–866, Aug. 2009.

[24] W. P. Ding et al., "A novel spark-based attribute reduction and neighborhood classification for rough evidence," *IEEE Trans. Cybern.*, vol. 54, no. 3, pp. 1470–1483, Mar. 2024.

[25] W. P. Ding, W. Pedrycz, I. Triguero, Z. H. Cao, and C. T. Lin, "Multigranulation supertrust model for attribute reduction," *IEEE Trans. Fuzzy Syst.*, vol. 29, no. 6, pp. 1395–1408, Jun. 2021.

[26] Y. J. Zhang, T. N. Zhao, D. Q. Miao, and W. Pedrycz, "Granular multilabel batch active learning with pairwise label correlation," *IEEE Trans. Syst., Man, Cybern. Syst.*, vol. 52, no. 5, pp. 3079–3091, May 2022.

[27] K. H. Yuan, D. Q. Miao, Y. Y. Yao, H. Y. Zhang, and X. R. Zhao, "Feature selection using zentropy-based uncertainty measure," *IEEE Trans. Fuzzy Syst.*, vol. 32, no. 4, pp. 2246–2260, Apr. 2024.

[28] S. Ding, H. Huang, J. Yu, and H. Zhao, "Research on the hybrid models of granular computing and support vector machine," *Artif. Intell. Rev.*, vol. 43, pp. 565–577, Apr. 2015.

[29] H. Liu and M. Cocea, "Granular computing-based approach for classification towards reduction of bias in ensemble learning," *Granular Comput.*, vol. 2, pp. 131–139, Nov. 2016.

[30] S. Butenkov, A. Zhukov, A. Nagorov, and N. Krivsha, "Granular computing models and methods based on the spatial granulation," *Procedia Comput. Sci.*, vol. 103, pp. 295–302, Jan. 2017.

[31] L. Chen, L. Zhao, Z. Xiao, Y. Liu, and J. Wang, "A granular computing based classification method from algebraic granule structure," *IEEE Access*, vol. 9, pp. 68118–68126, 2021.

[32] L. Chen, "Topological structure in visual perception," *Science*, vol. 218, no. 4573, pp. 699–700, Nov. 1982.

[33] G. Y. Wang, "DGCC: Data-driven granular cognitive computing," *Granular Comput.*, vol. 2, no. 4, pp. 343–355, Jul. 2017.

[34] S. Y. Xia, Y. S. Liu, X. Ding, G. Y. Wang, H. Yu, and Y. G. Luo, "Granular ball computing classifiers for efficient, scalable and robust learning," *Inf. Sci.*, vol. 483, pp. 136–152, May 2019.

[35] Y. F. Xue, Y. B. Shao, and H. Xia, "GBFSVM: A robust classification learning method," *Sci. J. Intell. Syst. Res.*, vol. 4, no. 1, pp. 238–245, Jan. 2022.

[36] S. Y. Xia, S. Y. Zheng, G. Y. Wang, X. B. Gao, and B. G. Wang, "Granular ball sampling for noisy label classification or imbalanced classification," *IEEE Trans. Neural Netw. Learn. Syst.*, vol. 34, no. 4, pp. 2144–2155, Apr. 2023.

[37] S. Y. Xia, X. C. Dai, G. Y. Wang, X. B. Gao, and E. Giem, "An efficient and adaptive granular-ball generation method in classification problem," *IEEE Trans. Neural Netw. Learn. Syst.*, vol. 35, no. 4, pp. 5319–5331, Apr. 2024.

[38] S. Y. Xia, X. Y. Lian, G. Y. Wang, X. B. Gao, J. C. Chen, and X. L. Peng, "GBSVM: An efficient and robust support vector machine framework via granular-ball computing," *IEEE Trans. Neural Netw. Learn. Syst.*, early access, Jul. 2, 2024, doi: 10.1109/TNNLS.2024.3417433.

[39] S. Y. Xia, H. Zhang, W. H. Li, G. Y. Wang, E. Giem, and Z. Z. Chen, "GBNRS: A novel rough set algorithm for fast adaptive attribute reduction in classification," *IEEE Trans. Knowl. Data Eng.*, vol. 34, no. 3, pp. 1231–1242, Mar. 2022.

[40] J. Yang et al., "3WC-GBNRS++: A novel three-way classifier with granular-ball neighborhood rough sets based on uncertainty," *IEEE Trans. Fuzzy Syst.*, vol. 32, no. 8, pp. 4376–4387, Aug. 2024.

[41] L. X. Zhao, Z. F. Zhang, W. J. Liu, and G. M. Lang, "GBTWSVM: Granular-ball twin support vector machine," in *Proc. Int. Joint Conf. Rough Sets*, Halifax, Canada, May 2024, pp. 238–251.

[42] Q. H. Zhang et al., "Incremental learning based on granular ball rough sets for classification in dynamic mixed-type decision system," *IEEE Trans. Knowl. Data Eng.*, vol. 35, no. 9, pp. 9319–9332, Sep. 2023.

[43] S. Y. Xia et al., "Ball k-means: Fast adaptive clustering with no bounds," *IEEE Trans. Pattern Anal. Mach. Intell.*, vol. 44, no. 1, pp. 87–99, Jan. 2022.

[44] J. Xie, W. Y. Kong, S. Y. Xia, G. Y. Wang, and X. B. Gao, "An efficient spectral clustering algorithm based on granular-ball," *IEEE Trans. Knowl. Data Eng.*, vol. 35, no. 9, pp. 9743–9753, Sep. 2023.

[45] D. D. Cheng, S. S. Liu, S. Y. Xia, and G. Y. Wang, "Granular-ball computing-based manifold clustering algorithms for ultra-scalable data," *Expert Syst. Appl.*, vol. 247, no. 1, Aug. 2024, Art. no. 123313.

[46] D. D. Cheng et al., "GB-DBSCAN: A fast granular-ball based DBSCAN clustering algorithm," *Inf. Sci.*, vol. 674, Jul.. 2024, Art. no. 120731.

[47] X. Ji, J. H. Peng, P. Zhao, and S. Yao, "Extended rough sets model based on fuzzy granular ball and its attribute reduction," *Inf. Sci.*, vol. 640, Sep. 2023, Art. no. 119071.

[48] S. Y. Xia, C. Wang, G. Y. Wang, X. B. Gao, E. Giem, and J. H. Yu, "GBRS: A unified model of Pawlak rough set and neighborhood rough set," *IEEE Trans. Neural Netw. Learn. Syst.*, vol. 36, no. 1, pp. 1719–1733, Jan. 2025.

[49] J. Yang et al., "Constructing three-way decision with fuzzy granular-ball rough sets based on uncertainty," *IEEE Trans. Fuzzy Syst.*, early access, Jan. 30, 2025, doi: 10.1109/TFUZZ.2025.3536564.

[50] X. L. Peng, P. Wang, S. Y. Xia, C. Wang, and W. Q. Chen, "VPGB: A granular-ball based model for attribute reduction and classification with label noise," *Inf. Sci.*, vol. 611, pp. 504–521, Sep. 2022.

[51] X. Y. Su, Z. Yuan, B. Y. Chen, D. Z. Peng, H. M. Chen, and Y. K. Chen, "Detecting anomalies with granular-ball fuzzy rough sets," *Inf. Sci.*, vol. 678, Sep. 2024, Art. no. 121016.

[52] W. B. Qian, W. Y. Ruan, Y. H. Li, and J. T. Huang, "Granular ball-based label enhancement for dimensionality reduction in multi-label data," *Appl. Intell.*, vol. 53, pp. 24008–24033, Jun. 2023.

[53] W. B. Qian, F. K. Xu, J. Qian, W. H. Shu, and W. P. Ding, "Multi-label feature selection based on rough granular-ball and label distribution," *Inf. Sci.*, vol. 650, Dec. 2023, Art. no. 119698.

[54] D. Y. Xia, G. Y. Wang, Q. H. Zhang, J. Yang, and S. Y. Xia, "Three-way approximations fusion with granular-ball computing to guide multigranularity fuzzy entropy for feature selection," *IEEE Trans. Fuzzy Syst.*, vol. 32, no. 10, pp. 5963–5977, Oct. 2024.

[55] L. Sun, H. B. Liang, W. P. Ding, and J. C. Xu, "Granular ball fuzzy neighborhood rough sets-based feature selection via multiobjective mayfly optimization," *IEEE Trans. Fuzzy Syst.*, vol. 32, no. 11, pp. 6112–6124, Nov. 2024.

[56] R. R. Yager and A. M. Abbasov, "Pythagorean membership grades complex numbers and decision making," *Int. J. Intell. Syst.*, vol. 28, no. 5, pp. 436–452, May 2013.

[57] R. R. Yager, "Pythagorean membership grades in multicriteria decision making," *IEEE Trans. Fuzzy Syst.*, vol. 22, no. 3, pp. 958–965, Aug. 2014.

[58] G. M. Lang, D. Q. Miao, and H. Fujita, "Three-way group conflict analysis based on Pythagorean fuzzy set theory," *IEEE Trans. Fuzzy Syst.*, vol. 28, no. 3, pp. 447–461, Mar. 2020.

[59] Y. Y. Yao, "The Dao of three-way decision and three-world thinking," *Int. J. Approx. Reasoning*, vol. 162, Nov. 2023, Art. no. 109032.

[60] M. Kelly, R. Longjohn, and K. Nottingham, "The UCI machine learning repository," 2023. [Online]. Available: https://archive.ics.uci.edu

Guangming Lang received the Ph.D. degree in mathematics from Hunan University, Changsha, China, in 2013.

He is currently a Professor with the School of Mathematics and Statistics, Changsha University of Science and Technology, Changsha. His main research interests include granular computing, rough set theory, fuzzy set theory, lattice theory, and three-way decision theory.

Lixi Zhao is currently working toward the M.S. degree in statistics with the School of Mathematics and Statistics, Changsha University of Science and Technology, Changsha, China.

Her main research interests include granular computing, granular-ball computing, fuzzy set theory, and three-way decision theory.

Duoqian Miao received the Ph.D. degree in pattern recognition and intelligent system from the Institute of Automation, Chinese Academy of Sciences, Beijing, China, in 1997.

He is currently a Professor with the School of Computer Science and Technology, and the Key Laboratory of Embedded System and Service Computing, Ministry of Education, Tongji University, Shanghai, China. His main research interests include rough sets, soft computing, machine learning, and intelligent systems.

Dr. Miao is a Fellow of International Rough Set Society and a Director of Chinese Association for Artificial Intelligence (CAAI). He is currently an Associate Editor for *Information Sciences*, *CAAI Transactions on Intelligence Technology*, *International Journal of Approximate Reasoning*, etc.

Weiping Ding (Senior Member, IEEE) received the Ph.D. degree in computer science from the Nanjing University of Aeronautics and Astronautics, Nanjing, China, in 2013.

He ranked within the top 2% ranking of scientists in the World by Stanford University (2020–2024). He has authored or coauthored more than 360 articles, including over 170 IEEE Transactions papers. He is currently a Professor with the School of Artificial Intelligence and Computer Science, Nantong University, Nantong, China, and also the Faculty of Data Science, City University of Macau, Macau, China. His main research interests include deep neural networks, granular data mining, and multimodal machine learning.

Dr. Ding serves as an Associate Editor/Area Editor/Editorial Board member of more than ten international prestigious journals, such as IEEE TRANSACTIONS ON NEURAL NETWORKS AND LEARNING SYSTEMS, IEEE TRANSACTIONS ON FUZZY SYSTEMS, *IEEE/CAA Journal of Automatica Sinica*, IEEE TRANSACTIONS ON EMERGING TOPICS IN COMPUTATIONAL INTELLIGENCE, IEEE TRANSACTIONS ON INTELLIGENT TRANSPORTATION SYSTEMS, IEEE TRANSACTIONS ON ARTIFICIAL INTELLIGENCE, *Information Fusion*, *Information Sciences*, *Neurocomputing*, *Applied Soft Computing*, *Engineering Applications of Artificial Intelligence*, *Swarm and Evolutionary Computation*, etc.